Case Studies in Thermal Engineering 68 (2025) 105865

Contents lists available at ScienceDirect

Case Studies in Thermal Engineering

journal homepage: www.elsevier.com/locate/csite

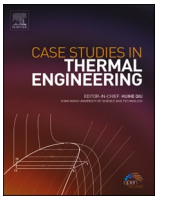

Thermal and radiative effects on unsteady MHD flow of Casson fluid past a rotating porous medium with variable mass diffusion

J. Prakash [a], A. Selvaraj [a,*], P. Ragupathi [b], Qasem M. Al-Mdallal [c], S. Saranya [c,**]

[a] Department of Mathematics, Vels Institute of Science, Technology & Advanced Studies, Chennai, 600117, Tamil Nadu, India
[b] Department of Mathematics, SRMV College of Arts and Science, Coimbatore, 641020, India
[c] Department of Mathematical Sciences, UAE University, Post Box -15551, Al-Ain, United Arab Emirates

ARTICLE INFO

Keywords:
MHD
Casson fluid
Rotating porous medium
Vertical plate
Variable mass diffusion
Laplace transform

ABSTRACT

This research examines the radiative components in heat and mass transfer phenomena in an unsteady MHD flow of Casson fluid past a vertical plate, set in a rotating porous medium. The fluid on the surface of the plate is maintained at a constant temperature while the mass transfer is set to vary. To examine the impact of heat generation, radiation, and variable mass diffusion on the velocity, temperature, and concentration profiles, the appropriate models are devised. The governing nonlinear partial differential equations are addressed through the use of Laplace transformations. The findings indicate that buoyancy forces imparted by the Grashof numbers considerably increase the velocity due to convection currents. However, the magnetic parameter counteracts velocity due to the Lorentz force while larger porosity increases fluid flow. Furthermore, radiation was demonstrated to decrease velocity and temperature from loss of heating while heat transfer increased temperature and velocity by injecting energy into the system. From the above results it can be seen that there are applications of these findings in the industrial and environmental context for example during MHD flow and filtration processes.

1. Introduction

Non-Newtonian fluids exhibit a complicated flow due to its viscosity being a function of shear rate. Some fluids, such as polymer solutions, gels, slurries, or blood, which fail to establish linearity in stress-strain relationship like Newtonian fluids, suffer from lack of linearity. When they are in the form of non-Newtonian fluids, getting through porous media, such as in filtration devices or systems, enhancing oil recovery or biomedical devices, these properties additionally influence the transport mechanisms for momentum, heat and mass transfer. The interplay between the rheological properties of the fluid and the pore geometry resulted in non-straight flow, making these systems difficult to model and forecast with accuracy. The investigation of non-Newtonian fluids confined to the pores has potentials in numerous fields. In petroleum engineering, for example, the understanding of the transport mechanisms as well as flow of non-Newtonian fluids, such as drilling muds, and enhanced oil recovery fluids, through fissured porous flows is significant for extraction enhancement. In environmental engineering, non-Newtonian fluids are applied for remediation works to mitigate contaminant transport in groundwater systems. Also, in the field of biomedical engineering, the flow of blood which is a non-Newtonian fluid through porous biomaterials is of great importance in the designing of tissue scaffolds for implants. It will assure

* Corresponding author.
** Corresponding author.
E-mail addresses: aselvaraj_ind@yahoo.co.in (A. Selvaraj), sannajshekar7@gmail.com (S. Saranya).

https://doi.org/10.1016/j.csite.2025.105865
Received 15 November 2024; Received in revised form 16 January 2025; Accepted 11 February 2025
Available online 13 February 2025

reasonable compatibility and proper nutrient transport. All of these applications emphasize non-Newtonian fluid modelling in porous media, which is efficient and desirable for various engineering and scientific systems. Recently, Ali et al. [1] explored an advanced approach to studying bioconvection phenomena using neural networks. The study focuses on heat and mass transfer characteristics in chemically reactive non-Newtonian nanofluids. Hakeem et al. [2] targeted the comparative thermal and flow characteristics of Newtonian and non-Newtonian basing fluids incorporating magnetic and non-magnetic nanoparticles. This comparison seeks to improve heat transfer augmentation, especially under conditions of a steady heat flux uniformly applied over a flat plat. Obi and Eze [3] formulated a mathematical model to study the effect of variation of viscosity with temperature on the flow and heat transfer in non-Newtonian incompressible and isothermal fluid passing through a cylinder. The results are useful in determining the optimization processes for the transportation of the non-Newtonian fluids in pipelines where temperature adjustments are needed to achieve the desired flow characteristics. Mehta et al. [4] looked into the conjugate heat transfer impacts on the thermo-hydraulic performance of non-Newtonian fluids in wavy solar channels. The study uses metallic porous blocks in the improvement of thermal conductivity and heat absorption with the aim of maximizing fluid flow and thermal efficiency in renewable energy systems. Bao et al. [5] pioneered an ANN-based, all-electronic control mechanism that is capable of modulating parameters of non-Newtonian fluid flow like viscosity and shear rate on demand, and this was possible thanks to the development of advanced electronic control on extremely complicated fluid flows using ANNs. Shah et al. [6] were successful in combining the Darcy-Forchheimer model of the porous media flow together with the Prandtl-Eyring non-Newtonian model. The authors provide an insight into the fluid behaviour in their diverse thermal conditions. Zaman et al. [7] have also looked into the plumes of magnetized trihybrid nanofluid drug carriers in blood flow for a stenosed artery over a magnetic field. The scope of the arteries may be altered as the nanofluid is concentrated onto the angiogenesis and its rheological properties alongside the magnetic field's effect in the flow of the blood due to the drug and nanofluid. Shah et al. [8] contributed to a more clear understanding of the flow of hybrid nanofluid in engine oil while incorporating the heat transfer and radiation effects while using the novel approach of Cattaneo–Christov heat flux model. Shah et al. [9] complemented the above work by considering multiple different aspects in the same case as an extension of the work. Such unique flow scenario that have been examined incorporates many complex factors in fluid dynamics and heat transfer including Darcy–Forchheimer MHD effects, rotational symmetry, micropolar fluid, and nanofluids. Khan et al. [10] conducted a comprehensive computational study of the flow of nanofluid blood in a stenosed artery. These authors have incorporated the effects of inflammation and viscous dissipation, which are important in the dynamics of blood flow in atherosclerotic conditions. Various studies on non-Newtonian fluid models are used to capture the flow characteristics of fluids of industrial interest such as Anwar et al. [11], Idowu and Falodun [12], Prameela et al. [13], Rehman et al. [14] and Abbas et al. [15].

The Casson type of fluids can be classified as non-Newtonian containing a yield stress which needs to be overcome followed by shear-thinning where viscosity is reduced as shear rate is increased. It was initially introduced to account for the flow of ink on the printing surface [16], which is now commonly used for modelling blood, chocolate, honey, polymers and other polymeric substances. Moreover Casson fluids also have wide applications. Its importance among non-Newtonian fluids lies in its capability to mimic dual effects of yield stress and shear thinning which makes it applicable widely for biological and industrial processes where both effects are of utmost importance. For example, considering the blood's flow characteristics, the Casson model is applicable in hemodynamic since it applies to small vessels and explains the character of blood flow which is dependent on turbulence viscosity and yield stress. In engineering applications, Casson fluids provide an understanding of flow behaviour characteristics of practice being a flow above a certain point is required and lock for processes involving more than one fluid the flow rate is of utmost importance. Due to their unique properties, Casson fluids are fundamentally important for modelling and optimizing numerous processes that require a greater degree of control over fluid dynamics. A number of case studies have been provided regarding Casson fluid flows in the past including that of Islam et al. [17] presented a model of magnetohydrodynamic (MHD) Casson fluid flow above an infinite vertical plate and included Brownian motion, thermophoretic effects and chemical reactions into the model. While modelling free convective Casson fluid flow through a permeable vertical plate with gyrotactic microorganisms, Usman et al. [18] sought to explain these microorganism's interaction with the flow and their migrative response to thermal and concentration gradient drives radicals. Mahmood et al. [19] studied Casson fluid flows over an infinite vertical Riga plate with slip boundary conditions and thermal radiation in its effects along with its effects in thermophoresis. Their combination aims to enhance flow control for cases of interest with slip borders and radiation heat transfer. In a different study, Hari Babu [20] considered heat and mass transfer in unsteady MHD Casson fluid flow past an infinite vertical porous plate in the presence of chemical reactions. His concentration was directed towards studying the joint action of the magnetic field and the chemical reacting process. Razzaq et al. [21] presented an innovative approach by integrating artificial intelligence (AI) with the analysis of magnetohydrodynamic (MHD) Casson nanofluid flows under the influence of chemical reactions and thermal radiation. More studies on fluid flow and heat transfer of Casson fluids can be found in Refs. [22–28].

Comprehending the flow characteristics above a vertical plate is significant in designing systems as it governs the efficiency with which heat and mass is transferred. The flow of fluid around a vertical plate is a prototypical problem of fluid movement that is done in a fluid mechanic setting which is moving fluid past an abutting vertical plane. In this model, a boundary layer is formed which means the fluid doesn't have any velocity at the surface of the plate, owing to the no-slip condition, and free-stream velocity further away from plate. Thermal and concentration boundary layers also develop depending on the temperature and concentration gradients between the plate and fluid. This arrangement is important as it represents a number of natural and industrial processes like cooling of electronic equipment, solar collectors and heat exchangers. Furthermore, looking at how the various layers within the fluid interact with the boundary layers and external features such as temperature, magnetic fields and surface roughness can assist engineers to performance of processes in different areas such as energy, environmental engineering among others. Padmaja and Rushi Kumar [29] studied the effects of viscous dissipation and chemical reactivity explicitly in MHD nanofluid flows over vertical plate in rotating systems. Khan et al. [30] studied unsteady MHD nanofluid over a vertical plate, slippery and permeable, in which memories were

incorporated through fractional-order derivatives. Some this work concerns the microscopic irreversible behaviour of nanofluid flow systems under magnetic and slip conditions, especially the role of fractional order derivatives in describing slippage effects on flow over permeable plates. Selvaraj et al. [31] observed that MHD parabolic flow past an accelerated vertical plate can account for heat and mass transfer in rotating frame. The study states that rotation influences the flow velocity as well as the momentum boundary layer of a flow field and diffusion of heat and mass increases the upper thermal and concentration profiles. Goud et al. [32] examined the role of thermal effects and viscous dissipation on MHD fluid flow when an accelerated vertical porous plate is placed in a stratified thermally controlled environment. The results obtained suggest that the thermal radiation increases the fluid temperature sufficiently which changes the stratification and thermal gradients and that viscous dissipation contributes more heat to the boundary layer. In recent times, many writers have made several proposals about the flow passed a vertical plate, as endorsed in Jose and Selvaraj [33], Raghunath et al. [34], Maran et al. [35], Kalita et al. [36] and Sudarmozhi et al. [37], Abrar et al. [38].

In general, radiation effects on fluid flow include the effects caused by the transfer of thermal radiation on the heat transfer as well as the behaviour of the fluid in the motion. Radiative heat transfer in a fluid flow implies that heat is not transferred only by conduction where the heat from the molecules of fluid is transmitted to other molecules or by convection where the heated fluid is transferred but also by electromagnetic waves. The added mode of heat transfer strongly modifies the temperature distribution within the fluid, in particular for high temperature environments or flows over heated boundaries. In many engineering and industrial applications, for example in nuclear reactors, combustion chambers, astrophysical flows or spacecraft thermal control, where radiation heat transfer can be more important than conduction or convection, radiation effects should not be disregarded. Radiation assists in the development of the boundary layer, determines thermal gradients of the fluid, and works together with the kinetic energy to determine thermal stability of the fluid. The correct design of radiation in liquids in motion makes it possible to use energy efficiently, to improve the cooling process, and to raise the energy stability limits of materials used in high-temperature conditions. Habib et al. [39] provided a sophisticated study that combines traditional fluid dynamics models with modern machine learning to optimize heat and mass transfer in chemically reactive nanofluids. More recent studies about the radiation effects can be found in Nandeppanavar [40], Lakshmikaanth et al. [41], Gumber et al. [42], Krishna et al. [43] and Kodi et al. [44]. Similarly, variable mass diffusion in fluid flow can be described as the situation when mass transfer takes place, however its rate is not constant and rather varies throughout space and time or is dependent on concentration gradient or properties of the temperature dependent mass transfer medium. This effect is significant in situations fluid flow over or through surfaces or medium with variable properties, for example in chemical reactors, natural flows, and biological systems. Concentration profiles get affected by variability in mass diffusion phenomena and may exhibit interaction between diffusion and convection within the boundary layer. Variable mass diffusion is crucial in flow systems modelling for processes that require strict control over concentration of species such as pollutant dispersal, catalytic reactions and transport of biomedically relevant nutrients. Considering spatially variable diffusion, engineers are able to estimate mixing and reaction rates as well as stability of mass transfer processes in numerous situations or applications. To this end, Nath et al. [45] researched to determine the effect of time-dependent temperature and periodic mass diffusion on the flow characteristics in the vicinity of a plate oscillating in the vertical direction. In particular it was observed that stratification has the effect of damping oscillations in these profiles which impact on the stability of flow characteristics in a substantial way. Nawaz et al. [46] focused on determining the contributions of partial slip and spatial non-uniformity of diffusion coefficient to mass and heat transfer rates in the context of chemical reaction influence. In particular results indicate that variable diffusion coefficient introduces non-uniform concentration profiles. Salahuddin et al. [47] examined the self induced effects of MHD forces on the flow of a Williamson fluid while keeping the electrical conductivity and diffusion effective variable. The study further sought the effects on heat and mass transfer characteristics of the system due to exponentially varying viscosity in the states space. Some of the most relevant studies ([48–51]) inspected the influence of variable thermal diffusion on vertical plate under various conditions.

Considering the industrial and engineering applications of rotating porous media under a magnetic field and their complex fluids, the analytic study of unsteady magnetohydrodynamic (MHD) flow of Casson fluid over a rotating porous medium is prevailing. Casson fluids that shear-thin with increasing shear rates and can be found in real-life applications such as blood, paints and several polymers solutions. While flowing through porous media, these fluids are expected to exhibit unique behaviour due to the combination of the fluid's rheology, magnetic field and porous matrix. The thermal radiation and the mass diffusion within the fluid affects the concentration and temperature distributions in the medium. These effects are critical in high temperature and chemically reacting systems like nuclear reactors, thermal energy storage, and catalytic systems. This study aims to investigate the combined influence of thermal radiation, heat generation, magnetic fields, and variable diffusion on Casson fluid flow, providing insights that are crucial for optimizing efficiency and stability in applications involving MHD flow over rotating, porous surfaces.

In particular, this work adds to the existing literature with respect to the unsteady MHD flow of Casson fluid past vertical plate embedded in a rotating porous medium by jointly investigating the effects of heat generation, and mass diffusion and radiation. It has been observed that previously performed studies have investigated either MHD flows of Casson fluids, but not jointly investigating the above said effects at the same time, this study bridges this gap. Our work integrates these aspects into a unified framework while also incorporating the influence of variable mass diffusion and rotating porous media. The uniqueness is primarily in the analytical solutions derived by means of Laplace transforms and the parametric analysis, which provides a new outlook into the optimization of heat and mass transfer processes in engineering and industrial equipment. This contribution is invaluable because it provides new basis for the understanding of the interplay of buoyancy, magnetic, and radiative forces in flow of complex fluids.

2. Casson fluid model

The Casson model is a rheological model commonly used to describe non-Newtonian fluids, particularly those that exhibit a yield

stress. This model was initially developed to describe the flow of materials like blood and chocolate, which do not flow until a certain threshold (yield stress) is exceeded. The rheological state for the Casson fluid model is represented as (see Ragupathi et al. [22]):

$$\tau^* = \tau_0 + \mu\beta^*,$$

(or)

$$\tau_{ij} = 2\begin{cases} \left(\mu_B + \frac{p_y}{\sqrt{2\Pi}}\right)e_{ij}, \Pi_c < \Pi, \\ \left(\mu_B + \frac{p_y}{\sqrt{2\Pi_c}}\right)e_{ij}, \Pi_c > \Pi, \end{cases}$$

where $\Pi = e_{ij}e_{ij}$ is the product of the component of the deformation rate; e_{ij} is the $(i,j)^{th}$ component of deformation rate; Π_c is the critical value of the product; μ_B is the plastic dynamic viscosity of the fluid; and $p_y = \mu_B\frac{\sqrt{2\Pi}}{\gamma}$ is the yield stress of the fluid.

3. Mathematical formulation of the problem

Consider the case of a Casson fluid stream that is moving through a porous medium while passing through an unending vertical plate (stiff). In this context, we take into consideration the $\widetilde{x}^*-$ axis, which is taken along the plate in a way that points up to the fluid flow, and the $\widetilde{y}^*-$ axis, which is taken in a normal direction into the plate. On an electrically conducting fluid that is perpendicular to the plate, a consistent magnetic field of strength B_0 is applied. At the beginning, when the time $\widetilde{t}^* \leq 0,$ is less than or equal to zero, both the plate and the fluid are in a state of rest. They are also kept at a constant temperature $\widetilde{T}^*_\infty$ and a constant surface concentration $\widetilde{C}^*_\infty$. With heat transfer starts of plate being lowered or raised to $\widetilde{T}^*_\infty + (\widetilde{T}^*_w - \widetilde{T}^*_\infty)\frac{\widetilde{t}}{t_0}$, the plate is given a parabolic motion $u_0\widetilde{t}^{*2}$; this motion occurs at a time when $\widetilde{t}^*$ is greater than or equal to zero. At a time $\widetilde{t}^*$ that is greater than or equal to zero, the concentration of the plate is either decreased or increased to $\widetilde{C}^*_\infty + (\widetilde{C}^*_w - \widetilde{C}^*_\infty)\frac{\widetilde{t}}{t_0}$. At a time when $\widetilde{t}^*$ is greater than or equal to zero, the constants $\widetilde{T}^*_w$ and $\widetilde{C}^*_w$ are maintained so that they remain constant.

To ensure controllability and to simplify the problem, several assumptions and approximations were made during the modelling process:

1. It is assumed that the fluid exhibits non-Newtonian behaviour, where the relationship between shear stress and shear rate is nonlinear.
2. It is assumed steady-state flow, meaning that the fluid's velocity and other flow properties do not change with time. Additionally, the fluid is considered incompressible, with a constant density and free convective.
3. We assume the existence of a boundary layer close to the surface of the cylinder. In this region, the flow is assumed to be primarily governed by viscous forces, and inertial effects are considered negligible.
4. For simplicity, we assume a small Reynolds number, implying that inertial forces are much smaller than viscous forces, which leads to a dominant viscous flow regime.
5. Higher-order effects, such as higher-order temperature gradients or small variations in velocity across the boundary layer, are often neglected.
6. We linearized certain nonlinear terms, particularly for the velocity or temperature profiles, to obtain analytical solutions or approximate numerical solutions.
7. We assume that the material properties, such as viscosity, thermal conductivity, and specific heat, are constant throughout the flow field.

In accordance with the aforementioned assumptions and taking into account Boussinesq's approximation, the partial differential equation that governs the situation with initial and boundary conditions is as follows (see Armstrong et al. [50] and Soundalgekar et al. [52]):

$$\frac{\partial\widetilde{u}^*}{\partial\widetilde{t}^*} = \nu\left(1+\frac{1}{\gamma}\right)\frac{\partial^2\widetilde{u}^*}{\partial\widetilde{y}^{*2}} + \frac{2\widetilde{\Omega}^*}{\rho}\widetilde{v}^* + g\beta_{\widetilde{T}^*}(\widetilde{T}^* - \widetilde{T}^*_\infty) + g\beta_{\widetilde{C}^*}(\widetilde{C}^* - \widetilde{C}^*_\infty) - \frac{\sigma B_0^2\widetilde{u}^*}{\rho} - \frac{\nu\phi\widetilde{u}^*}{k^*}, \tag{1}$$

$$\frac{\partial\widetilde{v}^*}{\partial\widetilde{t}^*} = \nu\left(1+\frac{1}{\gamma}\right)\frac{\partial^2\widetilde{v}^*}{\partial\widetilde{y}^{*2}} - \frac{2\widetilde{\Omega}^*}{\rho}\widetilde{u}^* - \frac{\sigma B_0^2\widetilde{v}^*}{\rho} - \frac{\nu\phi\widetilde{v}^*}{k^*}, \tag{2}$$

$$\frac{\partial\widetilde{T}^*}{\partial\widetilde{t}^*} = \frac{\kappa}{\rho c_p}\frac{\partial^2\widetilde{T}^*}{\partial\widetilde{y}^{*2}} - \frac{1}{\rho c_p}\frac{\partial q_r}{\partial\widetilde{y}^{*2}} + \frac{Q_1}{\rho c_p}(\widetilde{T}^* - \widetilde{T}^*_\infty), \tag{3}$$

$$\frac{\partial \widetilde{C}^*}{\partial \widetilde{t}^*} = Dm \frac{\partial^2 \widetilde{C}^*}{\partial \widetilde{y}^{*2}} . \tag{4}$$

The initial and boundary conditions for these equations are assumed as follows:

$$\begin{aligned}
&\widetilde{u}^* = 0, \widetilde{T}^* = \widetilde{T}^*_\infty, \widetilde{C}^* = \widetilde{C}^*_\infty, \text{for all } \widetilde{y}^* \geq 0, \widetilde{t}^* \leq 0, \\
&\widetilde{u}^* = \widetilde{u}_0 \widetilde{t}^{*2}, \widetilde{T}^* = \begin{cases} \widetilde{T}^*_\infty + \left(\widetilde{T}^*_w - \widetilde{T}^*_\infty\right) \dfrac{\widetilde{t}^*}{\widetilde{t}_0} & if \quad 0 < \widetilde{t}^* < \widetilde{t}_0 \\ \widetilde{T}^*_w & if\, \widetilde{t}^* \geq 0 \end{cases}, \\
&\widetilde{C}^* = \begin{cases} \widetilde{C}^*_\infty + \left(\widetilde{C}^*_w - \widetilde{C}^*_\infty\right) \dfrac{\widetilde{t}^*}{\widetilde{t}_0} & if \quad 0 < \widetilde{t}^* < \widetilde{t}_0 \\ \widetilde{C}^*_w & if\, \widetilde{t}^* \geq 0 \end{cases}, \\
&\widetilde{u}^* \to 0,\ \widetilde{T}^* \to \widetilde{T}^*_\infty,\ \widetilde{C}^* \to \widetilde{C}^*_\infty \quad as \quad \widetilde{y}^* \to \infty \ \text{and}\ \widetilde{t}^* \geq 0.
\end{aligned} \tag{5}$$

We simplify the radiative heat flux, q_r, using Rosseland approximation which is expressed as follows (see Reddy et al. [49]):

$$q_r = -\frac{4\sigma_r}{3\kappa_r} \left(\frac{\partial \widetilde{T}^{*4}}{\partial \widetilde{y}^*}\right), \tag{6}$$

where the κ_r indicates the mean absorption coefficient and σ_r indicates the Stefan Boltzmann constant respectively. Simplifying $\widetilde{T}^{*4}$ in Taylor's series about $\widetilde{T}^*_\infty$, ignoring higher order terms yields:

$$\widetilde{T}^{*4} \cong 4\widetilde{T}^{*3}_\infty \widetilde{T}^* - 3\widetilde{T}^{*4}_\infty . \tag{7}$$

Substitute equations (6) and (7) in equation (3) gives

$$\frac{\partial \widetilde{T}^*}{\partial \widetilde{t}^*} = \frac{\kappa}{\rho C_p} \frac{\partial^2 \widetilde{T}^*}{\partial \widetilde{y}^{*2}} + \frac{16\sigma_r \widetilde{T}^{*3}_\infty}{3\rho C_p \kappa_r} \left(\frac{\partial^2 \widetilde{T}^*}{\partial \widetilde{y}^{*2}}\right). \tag{8}$$

We make use of the following dimensionless variables in order to handle the dimensional PDE's given in Eqs. (1)–(4):

$$\left.\begin{aligned}
&\widetilde{y}^* = \widetilde{y}\widetilde{t}_0\widetilde{u}_0,\ \widetilde{t}^* = \widetilde{t}_0\widetilde{t},\ \widetilde{t}_0 = \frac{\nu}{\widetilde{u}_0^2},\ \widetilde{u}^* = \widetilde{u}_0\widetilde{U},\ \widetilde{v}^* = \widetilde{u}_0\widetilde{V}, \\
&\widetilde{T}^* = \widetilde{T}^*_\infty + \theta\left(\widetilde{T}^*_w - \widetilde{T}^*_\infty\right),\ \widetilde{C}^* = \widetilde{C}^*_\infty + \widetilde{C}\left(\widetilde{C}^*_w - \widetilde{C}^*_\infty\right)
\end{aligned}\right\}, \tag{9}$$

Using (9) in equations (1)–(4), we have derived

$$\frac{\partial \widetilde{U}}{\partial \widetilde{t}} = \left(1 + \frac{1}{\gamma}\right) \frac{\partial^2 \widetilde{U}}{\partial \widetilde{y}^2} + 2\Omega_1 \widetilde{V} + Gr\widetilde{T} + Gc\widetilde{C} - M\widetilde{U} - \frac{1}{K}\widetilde{U}, \tag{10}$$

$$\frac{\partial \widetilde{V}}{\partial \widetilde{t}} = \left(1 + \frac{1}{\gamma}\right) \frac{\partial^2 \widetilde{V}}{\partial \widetilde{y}^2} - 2\Omega_1 \widetilde{U} - M\widetilde{V} - \frac{1}{K}\widetilde{V}, \tag{11}$$

$$\frac{\partial \widetilde{T}}{\partial \widetilde{t}} = \frac{1}{Pr} \frac{\partial^2 \widetilde{T}}{\partial \widetilde{y}^2} - R\theta + Q\theta, \tag{12}$$

$$\frac{\partial \widetilde{C}}{\partial \widetilde{t}} = \frac{1}{Sc} \frac{\partial^2 \widetilde{C}}{\partial \widetilde{y}^2}. \tag{13}$$

Assuming the fluid velocity in complex form, $\widetilde{q} = \widetilde{U} + i\widetilde{V}$, we now pair equations (10) and (11) into a single equation as given below:

$$\frac{\partial \widetilde{q}}{\partial \widetilde{t}} = a \frac{\partial^2 \widetilde{q}}{\partial \widetilde{y}^2} + Gr\theta + Gc\widetilde{C} - m\widetilde{q}, \tag{14}$$

$$\frac{\partial\theta}{\partial\widetilde{t}}=\frac{1}{Pr}\frac{\partial^2\theta}{\partial\widetilde{y}^2}-R\theta+Q\theta, \tag{15}$$

$$\frac{\partial\widetilde{C}}{\partial\widetilde{t}}=\frac{1}{Sc}\frac{\partial^2\widetilde{C}}{\partial\widetilde{y}^2}, \tag{16}$$

where $a=\left(1+\frac{1}{\gamma}\right)$ and $m=M+2i\Omega_1+\frac{1}{K}$; also, we bring in below the dimensionless parameters:

$$\left.\begin{aligned}\gamma=\frac{\mu_\beta\sqrt{(2\pi c)}}{p_y},\Omega_1=\frac{\widetilde{\Omega}\nu}{\widetilde{u}_0^2},Gr=\frac{g\beta_{\widetilde{T}^*}\nu\left(\widetilde{T}_w^*-\widetilde{T}_\infty^*\right)}{\widetilde{u}_0^3},Gc=\frac{g\beta_{\widetilde{C}^*}\nu\left(\widetilde{C}_w^*-\widetilde{C}_\infty^*\right)}{\widetilde{u}_0^3},\\ M=\frac{\sigma B_0^2\nu}{\rho\widetilde{u}_0^2},K=\frac{\nu^2\phi}{k\,\widetilde{u}_0^2},Pr=\frac{\mu C_p}{k},R=\frac{16\sigma_r\widetilde{T}_\infty^3}{3\,\kappa\kappa_r\,u_0^2},Q=\frac{Q_1\nu}{\rho c_p\,u_0^2},Sc=\frac{\nu}{Dm}.\end{aligned}\right\}$$

Using the initial and boundary condition we get the following non dimensional quantities

$$\left.\begin{aligned}\widetilde{q}=0,\ \theta=0,\ \widetilde{C}=0,\ \text{for all}\ \widetilde{y}\geq 0\ \text{and}\ \widetilde{t}\leq 0\\ \widetilde{q}=\widetilde{t}^2,\ \ \theta=1,\ \ \widetilde{C}=\widetilde{t},\ for\ \widetilde{y}=0\ \text{and}\ \widetilde{t}>0\\ \widetilde{q}\to 0,\ \theta\to 0,\ \widetilde{C}\to 0,\ \ \text{as}\ \widetilde{y}\to\infty\text{and}\ \widetilde{t}>0\end{aligned}\right\} \tag{17}$$

4. Solution of the problem

equations (14)–(16) represent the dimensionless governing equations along with initial and boundary conditions which describe the behaviour of the system in study. In order to obtain analytical solutions, these equations can be addressed using the Laplace transform, which is a very effective mathematical technique which allows you to convert differential equations that depend on time into a Laplace domain. With the aid of Laplace transforms, we turn time-variant partial differential equations into algebraic equations which are in most instances comparatively easier to work with. After the transformations of the equations, they can be further operated on and solved in the Laplace domain. In the last place, the inverse Laplace transform allows us to transform the solutions of Laplace domain equations into the time domain. As a result, the received solutions are the solutions of described problem under given initial and boundary conditions. This approach yields the final analytical solutions for the specified initial and boundary conditions for the system as follows:

$$\widetilde{q}=\widetilde{q}_1+\widetilde{q}_2+\widetilde{q}_3+\widetilde{q}_4 \tag{18}$$

$$\theta=\frac{1}{2}\left[\begin{aligned}&e^{-2\eta\sqrt{P_r}\sqrt{(R-Q)\widetilde{t}}}erfc\left(\eta\sqrt{P_r}-\sqrt{(R-Q)\widetilde{t}}\right)\\&+e^{2\eta\sqrt{P_r}\sqrt{(R-Q)\widetilde{t}}}erfc\left(\eta\sqrt{P_r}+\sqrt{(R-Q)\widetilde{t}}\right)\end{aligned}\right] \tag{19}$$

$$\widetilde{C}=\widetilde{t}\left[\left(1+2\eta^2Sc\right)erfc\left(\eta\sqrt{Sc}\right)-\frac{2\eta\sqrt{Sc}}{\sqrt{\pi}}\exp\left(-\eta^2\mathrm{Sc}\right)\right] \tag{20}$$

where

$$q_1=\frac{\left(\eta^2+\left(\frac{m}{a}\right)\widetilde{t}\right)\widetilde{t}}{4\left(\frac{m}{a}\right)}\left[\begin{aligned}&\left(e^{2\eta\sqrt{\left(\frac{m}{a}\right)\widetilde{t}}}\,erfc\left(\eta+\sqrt{\left(\frac{m}{a}\right)\widetilde{t}}\right)+e^{-2\eta\sqrt{\left(\frac{m}{a}\right)\widetilde{t}}}\,erfc\left(\eta-\sqrt{\left(\frac{m}{a}\right)\widetilde{t}}\right)\right)\\&+\frac{\eta\sqrt{\widetilde{t}}\left(1-4\left(\frac{m}{a}\right)\widetilde{t}\right)}{8\left(\frac{m}{a}\right)^{\frac{3}{2}}}\left(\begin{aligned}&e^{-2\eta\sqrt{\left(\frac{m}{a}\right)\widetilde{t}}}\,erfc\left(\eta-\sqrt{\left(\frac{m}{a}\right)\widetilde{t}}\right)\\&-e^{2\eta\sqrt{\left(\frac{m}{a}\right)\widetilde{t}}}\,erfc\left(\eta+\sqrt{\left(\frac{m}{a}\right)\widetilde{t}}\right)\end{aligned}\right)-\frac{\eta\widetilde{t}}{2\left(\frac{m}{a}\right)\sqrt{\pi}}e^{-\left(\eta^2+\left(\frac{m}{a}\right)m\widetilde{t}\right)}\end{aligned}\right]$$

$$q_2=\frac{G_r}{b(1-aP_r)}\left[\begin{array}{c}\frac{1}{2}\left[e^{-2\eta\sqrt{\frac{m}{a}\tilde{t}}}erfc\left(\eta-\sqrt{\frac{m}{a}\tilde{t}}\right)+e^{2\eta\sqrt{\frac{m}{a}\tilde{t}}}erfc\left(\eta+\sqrt{\frac{m}{a}\tilde{t}}\right)\right]\\ -\frac{e^{bt}}{2}\left[\begin{array}{c}e^{-2\eta\sqrt{\left(\frac{m+b}{a}\right)\tilde{t}}}erfc\left(\eta-\sqrt{\left(\frac{m+b}{a}\right)\tilde{t}}\right)\\ +e^{2\eta\sqrt{\left(\frac{m+b}{a}\right)\tilde{t}}}erfc\left(\eta+\sqrt{\left(\frac{m+b}{a}\right)\tilde{t}}\right)\end{array}\right]\\ -\frac{1}{2}\left[\begin{array}{c}e^{-2\eta\sqrt{P_r}\sqrt{(R-Q)\tilde{t}}}erfc\left(\eta\sqrt{P_r}-\sqrt{(R-Q)\tilde{t}}\right)\\ +e^{2\eta\sqrt{P_r}\sqrt{(R-Q)\tilde{t}}}erfc\left(\eta\sqrt{P_r}+\sqrt{(R-Q)\tilde{t}}\right)\end{array}\right]\\ +\frac{e^{b\tilde{t}}}{2}\left[\begin{array}{c}e^{-2\eta\sqrt{P_r}\sqrt{(R+b-Q)\tilde{t}}}erfc\left(\eta\sqrt{P_r}-\sqrt{(R+b-Q)\tilde{t}}\right)\\ +e^{2\eta\sqrt{P_r}\sqrt{(R+b-Q)\tilde{t}}}erfc\left(\eta\sqrt{P_r}+\sqrt{(R+b-Q)\tilde{t}}\right)\end{array}\right]\end{array}\right]$$

$$q_3=\frac{G_m}{c^2(1-aS_c)}\left[\begin{array}{c}\frac{1}{2}\left[e^{-2\eta\sqrt{\frac{m}{a}\tilde{t}}}erfc\left(\eta-\sqrt{\frac{m}{a}\tilde{t}}\right)+e^{2\eta\sqrt{\frac{m}{a}\tilde{t}}}erfc\left(\eta+\sqrt{\frac{m}{a}\tilde{t}}\right)\right]\\ -\frac{e^{c\tilde{t}}}{2}\left[\begin{array}{c}e^{-2\eta\sqrt{\left(\frac{m+c}{a}\right)\tilde{t}}}erfc\left(\eta-\sqrt{\left(\frac{m+c}{a}\right)\tilde{t}}\right)\\ +e^{2\eta\sqrt{\left(\frac{m+c}{a}\right)\tilde{t}}}erfc\left(\eta+\sqrt{\left(\frac{m+c}{a}\right)\tilde{t}}\right)\end{array}\right]\\ -erfc\left(\eta\sqrt{Sc}\right)\\ +\frac{e^{c\tilde{t}}}{2}\left[\begin{array}{c}e^{-2\eta\sqrt{((Sc)c)\tilde{t}}}erfc\left(\eta\sqrt{Sc}-\sqrt{c\tilde{t}}\right)\\ +e^{2\eta\sqrt{((S_c)c)\tilde{t}}}erfc\left(\eta\sqrt{Sc}+\sqrt{c\tilde{t}}\right)\end{array}\right]\end{array}\right]$$

$$q_4=\frac{G_m}{c(1-aS_c)}\left[\begin{array}{c}\frac{1}{2}\left[e^{-2\eta\sqrt{\frac{m}{a}\tilde{t}}}erfc\left(\eta-\sqrt{\frac{m}{a}\tilde{t}}\right)+e^{2\eta\sqrt{\frac{m}{a}\tilde{t}}}erfc\left(\eta+\sqrt{\frac{m}{a}\tilde{t}}\right)\right]\\ -\frac{\eta\tilde{t}}{2\left(\frac{m}{a}\right)\sqrt{\pi}}\left(e^{-2\eta\sqrt{\frac{m}{a}\tilde{t}}}erfc\left(\eta-\sqrt{\frac{m}{a}\tilde{t}}\right)-e^{2\eta\sqrt{\frac{m}{a}\tilde{t}}}erfc\left(\eta+\sqrt{\frac{m}{a}\tilde{t}}\right)\right)\\ -\tilde{t}\left[(1+2\eta^2Sc)erfc\left(\eta\sqrt{Sc}\right)-\frac{2\eta\sqrt{Sc}}{\sqrt{\pi}}\exp\left(-\eta^2\mathrm{Sc}\right)\right]\end{array}\right]$$

where

$$erfc(a+ib)=\mathrm{erf}(a)+\frac{\exp\left(-a^2\right)}{2a\pi}[1-\cos(2ab)+isin(2ab)]\gamma+\frac{2\exp\left(-a^2\right)}{\pi}\sum_{n=1}^{\infty}\frac{\exp\left(-\eta^2/4\right)}{\eta^2+4a^2}[f_n(a,b)+ig_n(a,b)]+\in(a,b)$$

such that

$$f_n=2a-2a\,cos\,h(nb)\,cos\,(2ab)+n\,sin\,h\,(nb)\,sin\,(2ab)$$

$$g_n=2a\,cos\,h(nb)\,sin\,(2ab)+n\,sin\,h\,(nb)\,cos\,(2ab)$$

$$|\epsilon(a,b)| \approx \approx 10^{-16}|erf(a+ib)|$$

For the sake of simplicity, we have considered,

$$b = \frac{aP_r(R-Q)-m}{1-aP_r}, c = \frac{m}{aSc-1}, and\ \eta = \frac{\widetilde{y}}{2\sqrt{\widetilde{t}}}.$$

5. Results and discussion

In this section we present a detailed analysis of the radiative effects on heat and mass transfer within the unsteady MHD flow of Casson fluid across a rotating porous medium. Through variation of parameters like Casson fluid parameter (γ), thermal Grashof number (Gr), mass Grashof number (Gc), magnetic parameter (M), porosity parameter (K), heat generation (Q), radiation parameter (R) and Schmidt number (Sc), the effect of each factor on temperature, velocity and concentration profiles is assessed. The graphical results demonstrate the effect of these parameters on the thermal and concentration boundary layers and show some notable patterns or trends. Such understanding of the behaviour of the fluid under different conditions is crucial in order to tailor such systems for MHD flow systems in engineering applications.

5.1. Illustrations for velocity profile

In Fig. 1, the relation between the Casson parameter and the velocity profile, and more specifically its effect on the boundary layer has been depicted. However, since the Casson parameter increases, the amount of shear that the fluid can withstand increases as well. In the beginning, one could anticipate that the increase in resistance would reduce the velocity of the fluid close to the boundary of the layer and the reason being the fluid's high resistance to the applying shear forces. However, when the Casson parameter is increased, even the yield stress of the fluid goes up which allows the fluid to withstand more deformation before yield, thereby increasing the value of stress. Such yields stress compensation effects make it possible for the apparent wall shear stress to be larger. This results in lower induced velocity being developed along with a reduction in the angle with which higher Casson parameters become capable in developing suspensions. So, the Casson parameters have an inverse relation in the stability limit while showing more enhancement in the amount flow angle. From this, we reach a very important conclusion: with an increase of the Casson parameter the velocity increases along with the increase of the yield stress which comes in handy to counteract the resistance to the flow.

Fig. 2 showcases the effect of thermal Grashof number on the changes in the velocity profile. It is noticed that the velocity profile rises considerably. As seen, the increase in the thermal Grashof number indicates an increase in the temperature difference between the fluid layers and this causes an increase in buoyant forces to act in the warmer regions of the fluid and thus assists in movement. Therefore, as Gr values are consistently higher, it is expected that the velocity profile shows a greater value since more fluid is pushed, creating an increase in flow because of buoyancy forces. This has an even greater effect in natural convection where diversion forces such as pumps or fans are absent. In the case where the fluid is close to a heated surface, the elevation of Gr does certainly cause a rise in the velocity at the boundary because the less dense hot fluid rises and the much more dense cold fluid moves down to occupy space. This explains how a more steep velocity profile development can be observed as was shown in velocity profile analysis.

The outcomes of this study concerning effects of mass Grashof number are illustrated on Fig. 3. It is observed that not only the temperature gradients in the thermal Grashof number foster convection motion but concentration gradients in the mass Grashof number also increase the fluid motion which brings about a more complex velocity profile. As we move on stress, the mass Grashof number indicates that the denser fluid due to concentration gradients generates stronger buoyancy forces that cause thermal

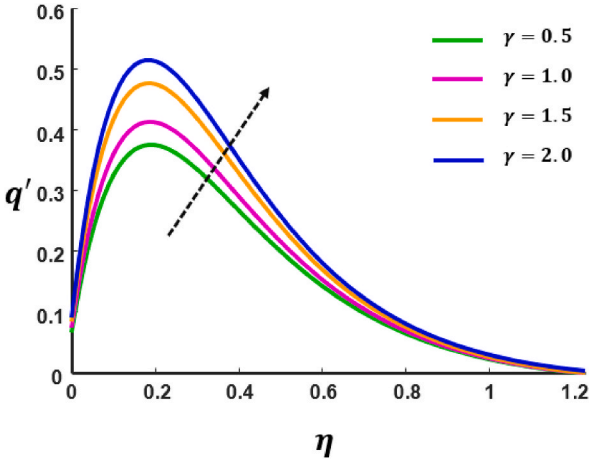

Fig. 1. Velocity profile variations for Casson parameter.

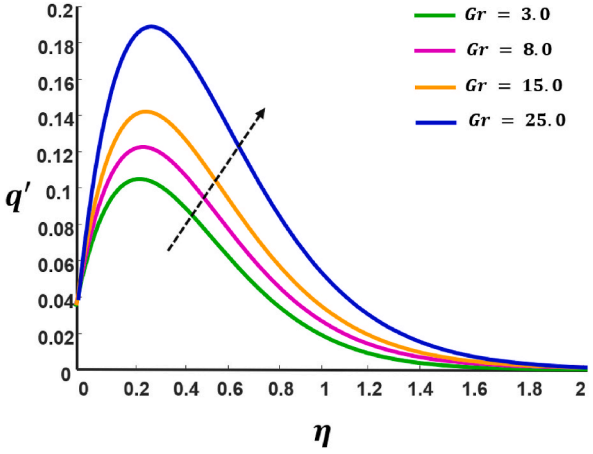

Fig. 2. Velocity profile variations for thermal Grashof number.

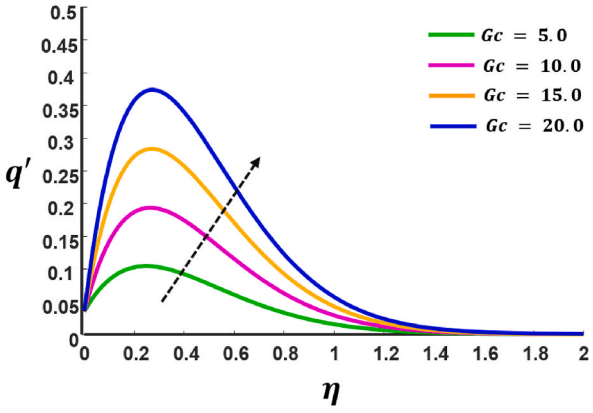

Fig. 3. Velocity profile variations for mass Grashof number.

convection and aid movement of fluids within the higher concentration zones compared to lower concentration zones. Therefore, the velocity profile is enhanced with an increase in *Gc*, as the concentration gradient buoyant force enhances the movement of the fluid.

The Lorentz force depends on the magnetic parameter and since it constitutes the velocity profile it is dependent on the strength of the magnetic field as well. In Fig. 4 it can be seen that the increase of the magnetic field strength leads to the remarkable slowdown of the magnetic parametric velocity profile. The magnetic Lorentz force acts normal to both the fluid motion and the magnetic field causing resistive forces acting against the movement of numerous particles in the fluid. The role of the bent Lorentz force is to serve as a damping mechanism of the shear stress which of course will eventually lead to the reduction of the fluid flow. This resistance leads to

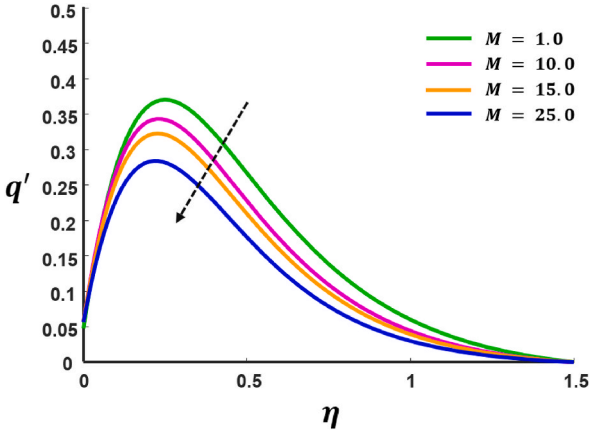

Fig. 4. Velocity profile variations for magnetic parameter.

the decrease of velocity where higher magnetic velocities could be seen to be reduced instead. As the strength of the magnetic field increases the depleting motion increases and as a result the fluids motion reduces. The electrically conducting fluid moves in the presence of a magnetic field. Due to such a fluid a race of charged particles are formed as a result particles experience a force due to the movement of particle which retards it. This has a drag type of effect, making even more the fluid motion slower. This behaviour can be considered as fundamental in applications that involve magnetic fields for the purpose of controlling or modifying fluid motion, and it brings out the importance of the magnetic parameter as an aid in controlling the motion of the fluid by limiting its free motion. Therefore, due to the increase of the magnetic parameter, the velocity profile is significantly reduced, and it perfectly exemplifies the effect of magnetic field on motion of fluid.

When the porosity parameter is increased, the inherent drag forces between the fluid and the solid particles of the medium is decreased, which directly facilitates better movement of the fluid allowing for a more robust and sharper velocity profile. Porous and permeable mediums have a more free flowing motion due to the less drag they have to experience, which helps reduce resistance. It is vital to mention that though the fluid has to exert some force against the solid particles of the medium, the interaction is greatly reduced and the permeability is improved. When the porosity parameter is increased, the permeability is enhanced and the medium in question offers even less resistance to the fluid. Hence due to the already reduced drag, when the fluid is forced to interact with the solid matrix in a porous structure, the medium permeability increases, leading to a faster flow and higher movement rate of the fluid, as shown in Fig. 5. As a result, an increase in porosity allows the fluid to meet less resistance and subsequently obtain a higher velocity profile. The impact is considerable for filtration systems, soils, or other porous materials systems because increasing the porosity permits for less fluid transport obstruction and thus more rapid velocity profiles. Therefore, a favorable flow through the increase in the porosity parameter is beneficial because the fluid meets less resistance within the medium which results in a more profound as well as a higher velocity profile.

A rising radiation parameter amplifies the intensity of heat transfer which in extreme scenarios can affect the thermal boundary layer of the fluid. This concept is effectively illustrated in Fig. 6 where an increase in the radiation parameter increases the absorbed saturates the energy within the fluid increasing its temperature gradient. As the temperature of the fluid is increased so too is the thermal effects on its viscosity which lowers the fluids resistance to flow. Due to this lowered viscosity shear stress at the boundary layer is lowered along with the vicinity of the surface hence increasing the fluid velocity. As the radiation parameter increases, it weakens the ability of the fluid to maintain its velocity especially close to the wall and the subsequent fall in the velocity profiles is noted.

From Fig. 7 it is evident that with deeper internal heat generation, the intensification of the velocity profile also takes place. The generated heat parameter means the internal heat within the fluid flow. The greater the heat generation parameter, the greater the temperature of the fluid which can be beneficial since it lowers the viscosity of the fluid. A low viscosity allows fluid particles to flow more freely resulting in faster movement across the fluid. This increase in movement brought forth by the reduction in viscosity leads to better transfer of momentum in a fluid, thus increasing the velocity of the fluid, especially at the boundary from the fluids.

According to the assessment made using Fig. 8, it shows that the higher the Schmidt number, the lower the velocity profile. When Schmidt number gets high, it means mass diffusion is taking place slower to momentum diffusion. This implies that the concentration boundary layer thickens as it increases in mass and therefore increases the resistance to flow of the fluid. This high resistance will lower the velocity of the fluid as a whole not only close to the surface but throughout the entire region of the fluid.

5.2. *Illustration for temperature profile*

Fig. 9 explains in detail the effect of the radiation parameter on the temperature profile. It is noted that with an increase in the values of the radiation parameter, the profile appears to be decreasing. With an increase in the radiation parameter, the fluid is able to absorb additional energy from the surrounding mediums via radiative transfer. However, this surplus radiative heat enhances the

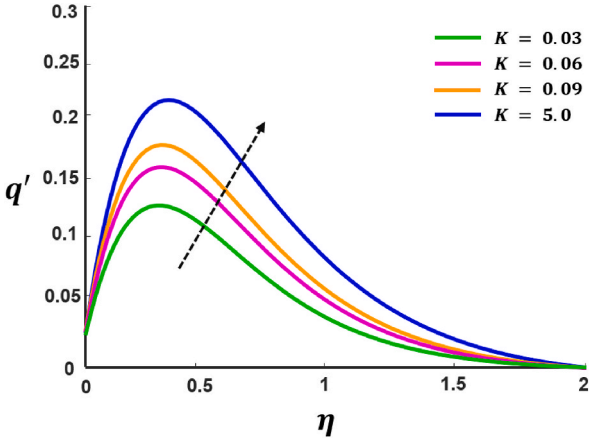

Fig. 5. Velocity profile variations for porosity parameter.

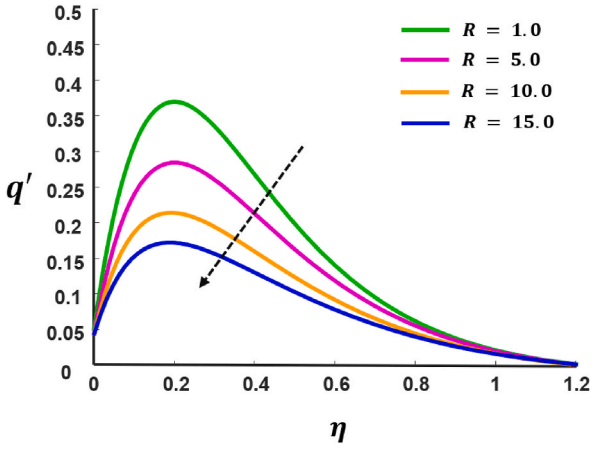

Fig. 6. Velocity profile variations for radiation parameter.

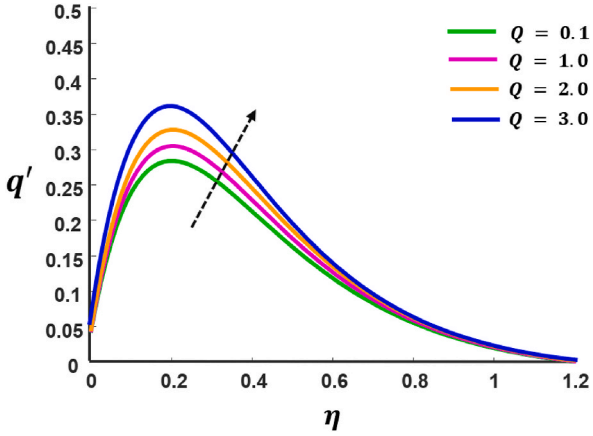

Fig. 7. Velocity profile variations for heat generation parameter.

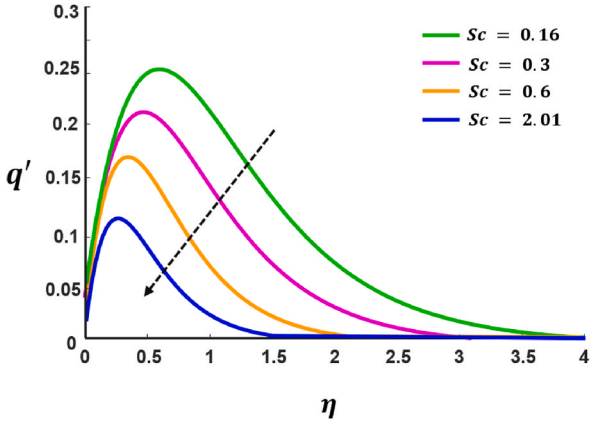

Fig. 8. Velocity profile variations for Schmidt number.

thermal energy of the fluid, which concentrates and causes a more homogeneous temperature distribution. It has been observed that when the radiation parameter increases, the temperature in regions closer to surface tends to the value or is even lower than it, this is due to the reason that the system becomes better at radiating the heat thus cutting down the temperature increase around the region.

With an increase in the heat generation parameter as shown in Fig. 10, the temperature profile is noted to become steeper with a

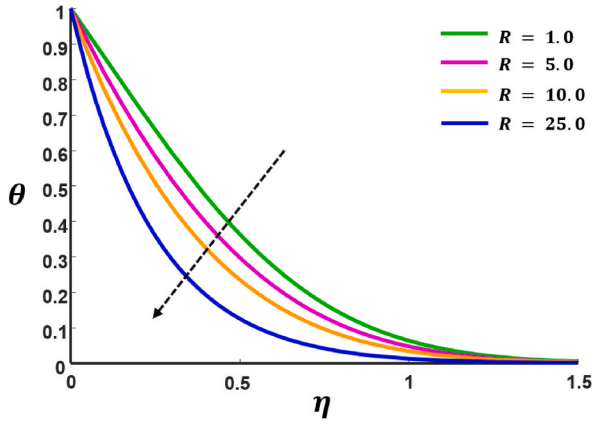

Fig. 9. Temperature profile variations for radiation parameter.

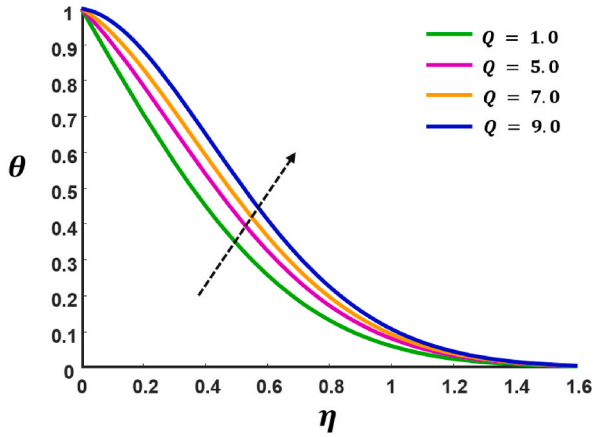

Fig. 10. Temperature profile variations for heat generation parameter.

higher temperature at the surface. The reason for this is because, as the heat generation parameter increases, more heat energy is introduced in to the system causing the fluid temperature to be raised. Due to this additional internal heat generation, the thermal energy of the fluid, more particularly the region close to the surface where heat is generated, will be elevated which in turn increases the temperature profile. Because heat is now continuously being applied to the fluid, the thermal boundary layer grows thicker as the fluid is able to gain more energy and the temperature within the surface region is raised.

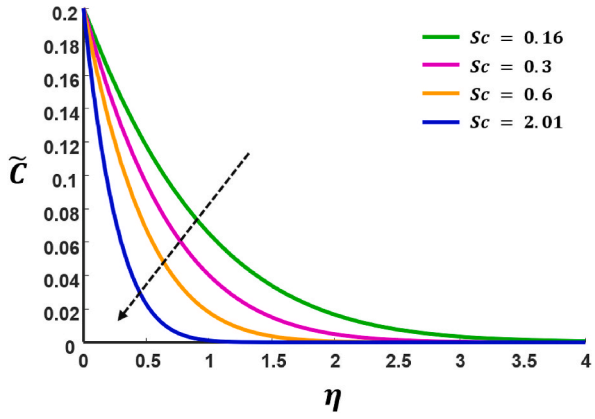

Fig. 11. Concentration profile variations for Schmidt number.

5.3. Illustration for concentration profile

Fig. 11 shows the effect of Schmidt number on the concentration profile. As can be seen, an increase in Schmidt number results in a lesser concentration of the overall concentration profiles. Essentially, an increase in the Schmidt implies that mass diffusivity is relatively low compared to the momentum diffusivity. This means that the concentration boundary layer which indicates the mass or concentration of a species in a fluid Gets thick. Thicker concentration of boundaries means that mass diffusion in regions of large target density is relatively slower in comparison to diffusion of species throughout the medium. This makes the change in concentration profile, with distance from the target wall, relatively steep. Hence, once a mass is concentrated at a boundary layer, diffusion in other areas of the solution is significantly less. Hence with increasing Schmidt number, the average concentration profile lowers while becoming more intense closer to the surface layer but further from the surface layer lowers the profile considerably due to being unable to diffuse across the boundary layer.

6. Conclusion

This research looks at the physics of fluid flow, heat and mass transfer for Casson fluid flowing over a vertical plate in porous medium under varying physical parameters. The differential equations governing the phenomena were algebraically manipulated using suitable mathematical methods and the findings were illustrated in graphs to show how these parameters affect the velocity, temperature and concentration profiles. The most important closing remarks are summarised as follows:

- An increase in the Casson parameter improves the velocity profile since fluids with low shear stress will not yield. In contrast, higher shear stresses will cause yielding, resulting in a steady and higher flow.
- Both the thermal and mass Grashof numbers enhance the velocity profile, indicating the influence of buoyancy forces driven by temperature and concentration gradients.
- The magnetic parameter was observed to have an adverse effect on the velocity profile. However, it was also noted that an increase in the porosity parameter improves the velocity profile, suggesting that a higher permeability of the porous matrix facilitates greater fluid movement.
- Increasing the radiation parameter leads to a decrease in the velocity profile, which is attributed to increased heat loss within the system.
- As the heat generation parameter increases, the velocity profile also increases, as the added thermal energy helps reduce the fluid's viscosity, thereby promoting fluid motion. Conversely, this also expands the temperature profile due to continuous heating in the system.
- Higher values of Schmidt numbers result in a reduction in the velocity profile due to an increase in mass diffusion resistance. Additionally, a rise in Schmidt numbers leads to a decrease in the concentration profile because mass diffusion is retarded.

7. Practical relevance

This study could prove useful in areas such as industrial heat management, geophysical fluid dynamics and chemical engineering processes. Examining features such as thermal and mass Grashof numbers, radiation and heat generation, have a potential in aiding the improvement of both heat and mass transfer in systems attached to porous and rotating surfaces, these include cooling technologies, filtration systems, and energy storing systems. For instance, the results illustrate that the variation of radiation and heat generation parameters can be used to improve the thermal efficiency of devices such as solar collectors and nuclear reactors. Moreover, the dependence of the velocity and temperature profiles on the magnitude of the magnetic parameter is important in the context of magnetohydrodynamic (MHD) pumps and flow control in electrically conducting fluids.

8. Future directions

Further elaboration to this work could be done by applying more complicated boundary conditions such as time varying heat flux or mixed convection to make the environment more realistic. This could potentially facilitate research on the behaviour of non-Newtonian fluids, which are often characterized by additional rheological attributes such as viscoelastic and shear thickening, and broaden the model's applications. Computational simulations and three-dimensional modelling would enhance comprehension of the spatial impact and transient dynamics, warranting wider applicability in industrial and environmental systems.

CRediT authorship contribution statement

J. Prakash: Writing – original draft, Methodology, Investigation, Formal analysis, Conceptualization. **A. Selvaraj:** Supervision, Methodology, Formal analysis, Conceptualization. **P. Ragupathi:** Writing – original draft, Visualization, Investigation, Formal analysis. **Qasem M. Al-Mdallal:** Visualization, Supervision, Investigation, Formal analysis. **S. Saranya:** Writing – original draft, Visualization, Investigation, Formal analysis.

Declaration of competing interest

The authors declare that they have no known competing financial interests or personal relationships that could have appeared to influence the work reported in this paper.

Acknowledgments

The authors wish to express their sincere thanks to the honorable referees and the editor for their valuable comments and suggestions to improve the quality of the paper. Additionally, all authors would like to express their gratitude to the United Arab Emirates University, Al Ain, UAE, for providing financial support with Grant No. 12R283.

Data availability

No data was used for the research described in the article.

References

[1] A. Ali, Z. Khan, M.B. Riaz, D. Gurram, M. Sun, A. Thaljaoui, Neural network analysis of bioconvection effects on heat and mass transfer in Non-Newtonian chemically reactive nanofluids, Case Stud. Therm. Eng. 64 (2024) 105534.
[2] A.A. Hakeem, S. Saranya, B. Ganga, Comparative study on Newtonian/non-Newtonian base fluids with magnetic/non-magnetic nanoparticles over a flat plate with uniform heat flux, J. Mol. Liq. 230 (2017) 445–452.
[3] B.I. Obi, F.C. Eze, Non-Newtonian fluid flow in an incompressible isothermal cylindrical pipe and temperature-dependent viscosity, Int J Res Sci Innovat. 11 (10) (2024) 74–81.
[4] S.K. Mehta, P.K. Mondal, S. Wongwises, Effect of conjugate heat transfer on thermo-hydraulic characteristics for non-Newtonian fluid flow in a wavy solar power plant with metallic porous blocks, AIP Conf. Proc. 3236 (1) (2024, October). AIP Publishing.
[5] H. Bao, X. Zhang, X. Zhang, X. Fan, J.W. Boley, J. Ping, Neural network–enabled, all-electronic control of non-Newtonian fluid flow, Appl. Phys. Lett. 125 (16) (2024).
[6] Z. Shah, A. Shafiq, M. Rooman, M.H. Alshehri, E. Bonyah, Darcy Forchhemier Prandtl-Eyring nanofluid flow with variable heat transfer and entropy generation using Cattaneo-Christov heat flux model: statistical approach, Case Stud. Therm. Eng. 49 (2023) 103376.
[7] T. Zaman, Z. Shah, M. Rooman, W. Khan, M.H. Alshehri, N. Vrinceanu, Rheological analysis of magnetized trihybrid nanofluid drug carriers in unsteady blood flow through a single-stenotic artery, Chin. J. Phys. 91 (2024) 538–559.
[8] Z. Shah, M. Rooman, M. Shutaywi, Computational analysis of radiative engine oil-based Prandtl–Eyring hybrid nanofluid flow with variable heat transfer using the Cattaneo–Christov heat flux model, RSC Adv. 13 (6) (2023) 3552–3560.
[9] Z. Shah, M. Sulaiman, A. Dawar, M.H. Alshehri, N. Vrinceanu, Darcy–Forchheimer MHD rotationally symmetric micropolar hybrid-nanofluid flow with melting heat transfer over a radially stretchable porous rotating disk, J. Therm. Anal. Calorim. (2024) 1–17.
[10] M.S. Khan, S. Ahmd, Z. Shah, M.H. Alshehri, E. Antonescu, Computational investigations of nanofluid blood flow in stenosed artery with effects of inflammation and viscous dissipation via finite element method, Chin. J. Phys. 92 (2024) 453–469.
[11] M.S. Anwar, M. Irfan, T. Muhammad, Non-Newtonian fluid flow over a stretching sheet in a porous medium with variable thermal conductivity under magnetohydrodynamics influence, ZAMM-J Appl Math Mech/Z Angew Math Mech. (2024) e202301048.
[12] A.S. Idowu, B.O. Falodun, Variable thermal conductivity and viscosity effects on non-Newtonian fluids flow through a vertical porous plate under Soret-Dufour influence, Math. Comput. Simulat. 177 (2020) 358–384.
[13] M. Prameela, K. Gangadhar, G.J. Reddy, MHD free convective non-Newtonian Casson fluid flow over an oscillating vertical plate, Part Differ Equ Appl Math. 5 (2022) 100366.
[14] S. Rehman, O.T. Bafakeeh, K. Guedri, Coupled energy and mass transport for non-Newtonian nanofluid flow through non-parallel vertical enclosure, Ain Shams Eng. J. 14 (8) (2023) 102023.
[15] N. Abbas, W. Shatanawi, T.A. Shatnawi, Theoretical analysis of modified non-Newtonian micropolar nanofluid flow over vertical Riga sheet, Int. J. Mod. Phys. B 37 (2) (2023) 2350016.
[16] N. Casson, A Flow Equation for Pigment-Oil Suspensions of the Printing Ink Type. Rheology of Disperse Systems, 1959.
[17] M.R. Islam, R. Biswas, M. Hasan, M. Afikuzzaman, S.F. Ahmmed, Modeling of MHD casson fluid flow across an infinite vertical plate with effects of brownian, thermophoresis, and chemical reactivity, Arabian J. Sci. Eng. (2024) 1–18.
[18] A. Usman, S.S. Abas, N.A. Jaafar, M.H. Muhammand, M. Mamat, A model on free convective casson fluid flow past a permeable vertical plate with gyrotactic microorganisms, J Adv Res Fluid Mech Thermal Sci. 105 (2) (2023) 31–50.
[19] Z. Mahmood, M.U. Rehman, K. Rafique, Adnan, U. Khan, S. Jubair, E.A. Ismail, F.A. Awwad, Time-dependent Casson fluid flow over a vertical Riga plate subjected to slip conditions and thermal radiation: aspects of Buongiorno's model, Adv. Mech. Eng. 16 (9) (2024) 16878132241283290.
[20] B. Hari Babu, Heat and mass transfer on unsteady MHD Casson fluid flow past an infinite vertical porous plate with chemical reaction, Proc. IME E J. Process Mech. Eng. 237 (6) (2023) 2278–2289.
[21] R. Razzaq, Z. Khan, M.N. Abrar, B. Almohsen, U. Farooq, Chemical reaction and radiation analysis for the MHD Casson nanofluid fluid flow using artificial intelligence, Chaos Solitons Fractals 190 (2025) 115756.
[22] P. Ragupathi, S. Saranya, H.V.R. Mittal, Q.M. Al-Mdallal, Computational study on three-dimensional convective casson nanofluid flow past a stretching sheet with arrhenius activation energy and exponential heat source effects, Complexity 2021 (1) (2021) 5058751.
[23] L. Liu, S. Zhang, S. Chen, C. Xie, L. Feng, A novel investigation of Casson fluid flow over an infinite plate with constant temperature by constructing the absorbing boundary conditions, Int. J. Heat Fluid Flow 107 (2024) 109404.
[24] U.J. Das, I. Patgiri, Effects of viscous dissipation, gravity modulation and Joule heating on MHD Casson fluid flow over a vertically moving plate with second-order slip velocity, Int. J. Ambient Energy 45 (1) (2024) 2331226.
[25] A.K. Sarma, D. Sarma, Unsteady magnetohydrodynamic bioconvection Casson fluid flow in presence of gyrotactic microorganisms over a vertically stretched sheet, Numer. Heat Tran., Part A: Applications (2024) 1–24.
[26] P. Vyas, Gajanand, Darcy-Forchhiemer thermofluidics of Micropolar-Casson fluid adjacent to a non-isothermal vertical plate with velocity slip using homotopy analysis method: Cattaneo-Christov flux, Numer. Heat Tran., Part B: Fundamentals (2023) 1–24.
[27] B.S. Goud, P. Srilatha, T. Srinivasulu, Y.D. Reddy, K.S. Kumar, Induced by heat source on unsteady MHD free convective flow of Casson fluid past a vertically oscillating plate through porous medium utilizing finite difference method, Mater. Today Proc. (2023), https://doi.org/10.1016/j.matpr.2023.01.378.
[28] M.D. Shamshuddin, R.P. Sharma, A. Ghaffari, S.R. Allipudi, Induced magnetic transportation of Soret and dissipative effects on Casson fluid flow towards a vertical plate with thermal and species flux conditions, Int. J. Mod. Phys. B 38 (11) (2024) 2450157.
[29] K. Padmaja, B. Rushi Kumar, Viscous dissipation and chemical reaction effects on MHD nanofluid flow over a vertical plate in a rotating system, ZAMM-J Appl Math Mech/Z Angew Math Mech. 103 (9) (2023) e202200471.

[30] Z.H. Khan, O.D. Makinde, M. Usman, R. Ahmad, W.A. Khan, Z. Huang, Inherent irreversibility in unsteady magnetohydrodynamic nanofluid flow past a slippery permeable vertical plate with fractional-order derivative, J Comput Design Eng. 10 (5) (2023) 2049–2064.
[31] A. Selvaraj, S.D. Jose, R. Muthucumaraswamy, S. Karthikeyan, MHD-parabolic flow past an accelerated isothermal vertical plate with heat and mass diffusion in the presence of rotation, Mater. Today Proc. 46 (2021) 3546–3549.
[32] B.S. Goud, P. Srilatha, D. Mahendar, T. Srinivasulu, Y.D. Reddy, Thermal radiation effect on thermostatically stratified MHD fluid flow through an accelerated vertical porous plate with viscous dissipation impact, Part Differ Equ Appl Math. 7 (2023) 100488.
[33] S.D. Jose, A. Selvaraj, Convective heat and mass transfer effects of rotation on parabolic flow past an accelerated isothermal vertical plate in the presence of chemical reaction of first order, JP J. Heat Mass Transf. 24 (1) (2021) 191–206.
[34] K. Raghunath, M. Obulesu, K. Venkateswara Raju, Radiation absorption on MHD free conduction flow through porous medium over an unbounded vertical plate with heat source, Int. J. Ambient Energy 44 (1) (2023) 1712–1720.
[35] D. Maran, A. Selvaraj, M. Usha, S. Dilipjose, First order chemical response impact of MHD flow past an infinite vertical plate with in the sight of exponentially with variable mass diffusion and thermal radiation, Mater. Today Proc. 46 (2021) 3302–3307.
[36] N. Kalita, R.K. Deka, R.S. Nath, Unsteady flow past an accelerated vertical plate with variable temperature in presence of thermal stratification and chemical reaction, East Eur J Phys. (3) (2023) 441–450.
[37] K. Sudarmozhi, D. Iranian, I. Khan, A. S. Al-johani, S.M. Eldin, Magneto radiative and heat convective flow boundary layer in Maxwell fluid across a porous inclined vertical plate, Sci. Rep. 13 (1) (2023) 6253.
[38] M.N. Abrar, R. Razzaq, N. Islam, Z. Khan, K. Irshad, Analyzing slip factor impacts on bio-convective micro-rotating nanofluids over a stretchable plate: an artificial neural network approach, Chaos Solitons Fractals 188 (2024) 115537.
[39] S. Habib, S. Nasir, Z. Khan, A.S. Berrouk, W. Khan, S. Islam, Optimization of heat and mass transfer in chemically radiative nanofluids using Cattaneo-Christov fluxes and advanced machine learning techniques, Ain Shams Eng. J. 15 (12) (2024) 103129.
[40] M.M. Nandeppanavar, K. Mc, R. N, Effect of non-linear thermal radiation on the stagnation point flow of double diffusive free convection due to movingvertical plate, J. Eng. Des. Technol. 21 (1) (2023) 150–166.
[41] D. Lakshmikaanth, A. Selvaraj, P. Selvaraju, S.D. Jose, Hall and heat source effects of flow past a parabolic accelerated isothermal vertical plate in the presence of chemical reaction and radiation, JP J. Heat Mass Transf. 34 (2023) 105–126.
[42] P. Gumber, M. Yaseen, S.K. Rawat, M. Kumar, Heat transfer in micropolar hybrid nanofluid flow past a vertical plate in the presence of thermal radiation and suction/injection effects, Part Differ Equ Appl Math. 5 (2022) 100240.
[43] M.V. Krishna, N.A. Ahamad, A.J. Chamkha, Radiation absorption on MHD convective flow of nanofluids through vertically travelling absorbent plate, Ain Shams Eng. J. 12 (3) (2021) 3043–3056.
[44] R. Kodi, O. Mopuri, S. Sree, V. Konduru, Investigation of MHD Casson fluid flow past a vertical porous plate under the influence of thermal diffusion and chemical reaction, Heat Trans. 51 (1) (2022) 377–394.
[45] R.S. Nath, H. Kumar, R.K. Deka, Theoretical investigation of thermal and mass stratification effects on unsteady flow across a vertical oscillating plate with periodic temperature variation and variable mass diffusion, Heat Trans. 53 (7) (2024) 3605–3624.
[46] M. Nawaz, S. Rafiq, I.H. Qureshi, S. Saleem, Combined effects of partial slip and variable diffusion coefficient on mass and heat transfer subjected to chemical reaction, Phys. Scri. 95 (3) (2020) 035222.
[47] T. Salahuddin, M. Khan, T. Saeed, M. Ibrahim, Y.M. Chu, Induced MHD impact on exponentially varying viscosity of Williamson fluid flow with variable conductivity and diffusivity, Case Stud. Therm. Eng. 25 (2021) 100895.
[48] M. Farooq, S. Ahmad, M. Javed, A. Anjum, Analysis of Cattaneo-Christov heat and mass fluxes in the squeezed flow embedded in porous medium with variable mass diffusivity, Results Phys. 7 (2017) 3788–3796.
[49] B.P. Reddy, O.D. Makinde, A. Hugo, A computational study on diffusion-thermo and rotation effects on heat generated mixed convection flow of MHD Casson fluid past an oscillating porous plate, Int. Commun. Heat Mass Tran. 138 (2022) 106389.
[50] A.N. Armstrong, N. Dhanasekar, A. Selvaraj, R. Shanmugapriya, P.K. Hemalatha, J.N. Kumar, Rotational effect of parabolic flow past in a vertical plate through porous medium with variable temperature and uniform mass diffusion, AIP Conf. Proc. 2821 (1) (2023, November). AIP Publishing.
[51] R. Ayub, S. Ahmad, M. Ahmad, MHD rotational flow of viscous fluid past a vertical plate with slip and Hall effect through porous media: a theoretical modelling with heat and mass transfer, Adv. Mech. Eng. 14 (6) (2022) 16878132221103330.
[52] V.M. Soundalgekar, S.K. Gupta, N.S. Birajdar, Effects of mass transfer and free convection currents on MHD Stokes' problem for a vertical plate, Nucl. Eng. Des. 53 (3) (1979) 339–346.